RESEARCH ARTICLE

Macromolecular Materials and Engineering
Open Access
www.mame-journal.de

Mycelium Agrowaste-Bound Biocomposites as Thermal and Acoustic Insulation Materials in Building Construction

*Kumba Bintunia Bonga, Laura Bertolacci, Marco Contardi, Uttam Chandra Paul, Muhammad Shajih Zafar, Giorgio Mancini, Lara Marini, Luca Ceseracciu, Despina Fragouli, and Athanassia Athanassiou**

The predominant use of synthetic materials, such as fiberglass and polymeric foams, for thermal and acoustic insulation in the construction sector contributes to the recalcitrant waste accumulation in the environment and is not economically sustainable in the long term. This is because they are developed with linear economy standards, they are neither reusable nor recyclable, and, at their end of lifecycle, they are not compostable, with a great amount of them finishing in landfills. This work is focused on the development of natural, self-growing mycelium-biocomposites as sustainable alternatives to these conventional synthetic materials. Specifically, fungal mycelium derived from the nonpathogenic fungal strain *Pleurotus ostreatus* is fed by coffee silverskin flakes, a lignocellulosic agrowaste from roasted coffee seeds, forming 3D biocomposites. The physicochemical properties of the obtained composite are thoroughly investigated, with a final focus on their thermal and acoustic insulation properties. As proved, the natural agrowaste-mycelium composites possess high porosity and thus low density, good thermal properties, and satisfactory sound absorption capability. Such properties combined with the minimal energetic requirements for their growth and their fully compostable end-of-life nature make them valuable alternatives for thermal and acoustic insulation in building construction, among other applications, promoting environmental and economic sustainability.

1. Introduction

According to a 2022 United Nations report, the buildings and construction sector is not on track to reach the decarbonization target by 2050.[1,2] The sector accounted for about 37% of energy and process-related CO_2 emissions in 2021, 11% of which was emitted during building materials manufacturing.[2] For this reason, the focus of the building industry has recently been directed toward the development of bio-based materials to be used in the construction of eco-friendly building structures, in compliance with environmental policies to reduce the adverse impacts on the environment.[3]

At the moment, traditional polymeric foams, such as polystyrene and polyurethane, rock mineral wool, and fiberglass are commonly used for thermal insulation of public and private buildings in temperate climate regions.[4,5] On the other hand, for acoustic insulation, porous and fiber-based materials such as polyurethane foams, fiberglass fabrics, metallic frames, etc., applied usually as panels to walls, floors, and ceilings are widely used.[6,7] Although such materials can sufficiently isolate buildings from heat and sound creating a comfortable and safe internal ambient, most of them present several limitations in terms of their recycling and reuse,[8,9] and they are nonbiodegradable, excluding the composting end-of-life. On top, their production involves complex manufacturing processes and

K. B. Bonga, L. Bertolacci, M. Contardi, U. C. Paul, M. S. Zafar, G. Mancini, L. Marini, D. Fragouli, A. Athanassiou
Smart Materials
Istituto Italiano di Tecnologia
via Morego 30, Genova 16163, Italy
E-mail: athanassia.athanassiou@iit.it

The ORCID identification number(s) for the author(s) of this article can be found under https://doi.org/10.1002/mame.202300449

DOI: 10.1002/mame.202300449

K. B. Bonga
Dipartimento di Informatica, Bioingegneria, Robotica e Ingegneria dei Sistemi (DIBRIS)
Università di Genova
via Opera Pia 13, Genova 16145, Italy

M. Contardi
Department of Earth and Environmental Sciences (DISAT)
Piazza della Scienza
Milan 20126, Italy

L. Ceseracciu
Materials Characterization Facility
Istituto Italiano di Tecnologia
via Morego 30, Genova 16163, Italy

substantial energy consumption.[10–15] Finally, when exposed to harsh conditions such as accidental fire, they may leach out hazardous substances, such as carbon monoxide, hydrogen cyanide, isocyanates, etc.,[14,16,17] raising a well-documented environmental health problem.[18,19]

Thermal and acoustic insulation components based on biodegradable and bio-based materials, which commonly require less energy to be produced and transformed than the traditional systems,[20] are economically as well as environmentally sustainable alternatives to their synthetic counterparts. The utilization of bio-based engineered building insulation materials acts against the over-exploitation of depleting natural resources,[21] and is a vital mitigation strategy to achieve environmentally safe solutions, decreasing the threats of plastic pollution to the environment.[22,23] To this end, among the various biomaterials, agrowaste-based mycelium biocomposites can be the ideal alternatives. Such materials derive from renewable resources, and on the top, their development occurs with minimal energy requirements due to their self-growing nature. Importantly, they are compostable under environmental conditions at the end of their lifecycle.[24–26] In particular, recent studies have shown that mycelium biocomposites are biodegradable, they can act as CO_2-sink, while compared to other systems the energy required for their fabrication is 1.5–6 time less, and they have lower impact on water consumption, particles emission and on the overall climate change.[27]

In particular, mycelium, the vegetative part of fungi, is a network of branching, tube-like filaments called hyphae that in nature grow underneath the ground.[28] Fibrous mycelium networks can grow in a cost effective way using natural substrates as feedstock, and depending on the conditions they may form 2D fibrous mats,[29–33] or 3D porous constructs.[34] Therefore, various mycelium strains, including *Ganoderma lucidum*, *Pleurotus ostreatus (P. ostreatus)*, *Trametes versicolor*, *Schizophyllum commune*, and *Agaricus bisporus*, grown on wood by-products or agricultural waste such as, wood chips, sawdust, straw, and other organic materials, molded into different shapes, have been proposed for components in furniture,[35] accessories,[35] fabrics,[36,37] and in packaging materials among others.[35,36,38]

Mycelium has also inherent insulating properties,[12,39] since its filamentous network creates a dense 3D structure with interconnected pores and appropriate porosity, density, pores structure, and filaments dimensions for such types of application. Such materials have been proposed as barriers to the external stimuli such as the temperature variations[40] or the sound waves transmission.[7,12,41–43] In particular, mycelium was found to be an exceptional acoustic absorber of the mid-low-frequencies (< 1500 Hz).[12,42] Indeed, in the field of insulation, different mycelia species have been combined with various types of agrowaste, to grow panels and bricks for insulation applications and they have shown good thermal and acoustic properties satisfying the construction needs.[12,39,40,44,45] Characteristic examples are *Ganoderma resinaceum* combined with miscanthus giganteus fibers,[46] *P. ostreatus* grown on combined rice hulls, birch sawdust and rye grain,[47] or on bagasse,[48] coconut husk,[49] rice husk,[49–51] juncao grass,[49] sawdust,[51] and cotton,[52,53] *Trametes versicolor* grown on oak heartwood,[54] or on sawdust in combination with *Ganoderma lucidum*,[45] and *Trametes multicolor* cultivated on straw.[52,53]

However, the type of agrowaste substrate and mycelium strain chosen affect not only the insulation's performance but also the overall properties of the end product and its scalability.[12,53,55] Indeed, principal limitations are related to unsuitable mechanical properties of the final mycelium-agrowaste structure, to the limited availability of the chosen agrowaste substrate or to the slow growth rate of some mycelium strains, which restrict their feasibility for large-scale construction projects. To become a competitive alternative to the commercially available insulating materials, investments on large scale incubators and research on scaled up controlled growth using abundant agrowaste components are needed. In this research work, we used the *P. ostreatus* strain which grows fast on natural substrates, including lignocellulosic agrowastes. A byproduct of the coffee industry, namely coffee silverskin flakes (CSF), was used as the growing substrate. CSF is the outer layer surrounding the green coffee beans, released when they are roasted, and is the only by-product of the roasting process.[56] It represents 4% w/w of the coffee bean, and considering that about 10 million tons of coffee beans are processed annually, about 400 thousand tons of CSF are generated each year in the coffee roasting industry.[57,58] It is mainly composed of cellulose and lignin and due to its abundance and availability, is an attractive and renewable resource to develop composites for various applications.[59]

In particular, in this study we present for the first time the cost-effective and self-growing production of 3D porous biocomposite materials, through the combination of CSF with *P. ostreatus* mycelium, with mechanical characteristics and thermal and acoustic insulation properties suitable for the building construction industry. Among the various combinations studied, the initial weight ratio of (1:5) agrowaste: mycelium promotes the most efficient mycelial growth colonization on CSF within a week period and results in composites with the highest sound absorption capability. The developed biocomposites also exhibit low thermal conductivity comparable with conventional insulation materials. This is an advancement in the state of the art of the biocomposites for the building sector deriving from renewable, affordable, and easily accessible resources, with minimal energy requirements for their development.

2. Results and Discussion

The photographs of the biocomposites derived from the various CSF to mycelia weight ratios are shown in **Figure 1**. The images indicate a successful growth of the *P. ostreatus* mycelium within and around the CSF since the whitish mycelial colonization can be observed throughout the samples. Notably, the mycelium component in the final composite samples increases, as the mycelium inoculum in the initial composition increases (from 1:1 to 1:5 CSF: mycelia weight ratio, CSF:P). This observation is further confirmed by the SEM analysis where the microstructure of the fibrous mycelium within the biocomposites was evaluated. Indeed, as shown in the SEM images of the dried samples, in **Figure 2**, the nondirectional growth of the mycelium filaments (of a few μm diameter), form an interconnected fibrous network in between and around the CSF particles. Such network results in a 3D porous structure comprising air pockets formation. This filamentous network becomes denser as the amount

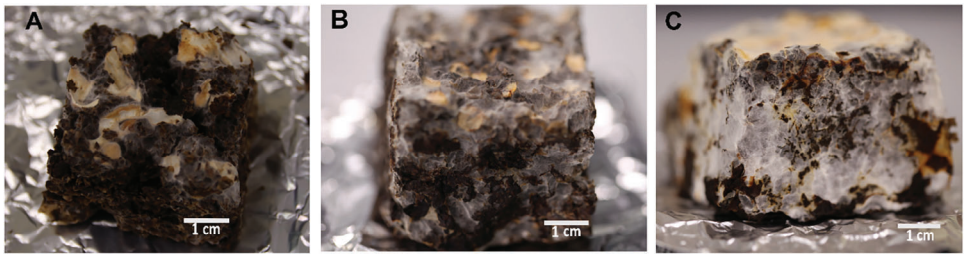

Figure 1. Photographs of the 3D biocomposite samples with initial weight ratios CSF/P 1:1 (3 × 4 × 2 cm^3) A), 1:2 (2 × 5 × 3 cm^3) B), and 1:5 (2 × 5 × 4 cm^3) C). The initial ratio between the mycelium and the biomass used for its growth clearly affects the morphology of the final samples after 1 week of growth.

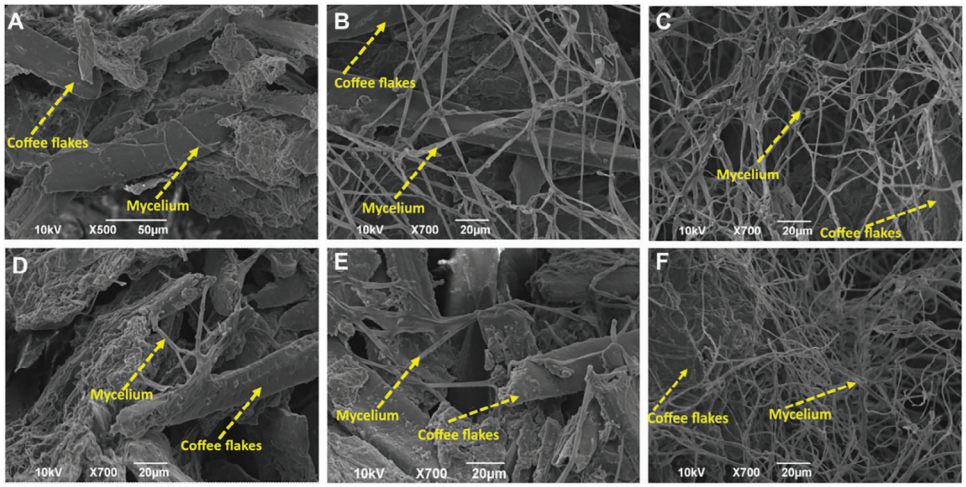

Figure 2. Morphological characterizations. A–C) Surface and D–F) Cross-sectional SEM images of the CSF/P 1:1 A,D), 1:2 B,E), and 1:5 C,F) samples, showing the morphological differences between them.

of the mycelium inoculum in the initial composition increases, resulting in a better-defined fibrous 3D network.

The mercury intrusion porosimetry (MIP) analysis was performed, in order to determine the porosity and the pore size distribution of the developed 3D biocomposites, focusing on those with the highest amount of mycelium fibers (CSF/P 1:5). As shown in **Figure 3**A, the biocomposites pores' size distribution is broad, with around 80% of the cumulative pore volume attributed to pores with diameter between 3.6 and 100.0 μm, while the overall porosity is 53.46%.

The *P. ostreatus* mycelium mats grown on PDB, the pristine CSF, and the produced biocomposites were analyzed by attenuated total reflectance-fourier transform infrared spectroscopy (ATR-FTIR), and the results are reported in Figure 3B. The spectrum of *P. ostreatus* (black line) presents the typical bands of the O—H and N—H stretching modes between 3500 and 3100 cm^{-1}, attributed to the protein and saccharide components and the adsorbed humidity; the asymmetric and symmetric CH_2 and CH_3 stretching modes at 2955, 2918, 2876, and 2851 cm^{-1} are due to the lipidic part of the mycelium; the amide I and amide II stretching modes centered at 1641 and 1541 cm^{-1} are attributed to the proteins of the mycelium, while the C—O and C—O—C stretching modes between 1200 and 1000 cm^{-1} are typical of polysaccharides.[29,55]

At the spectrum of CSF (red line) the O—H and N—H stretching modes between 3500 and 3100 cm^{-1} are also related to adsorbed humidity, protein, and saccharide components; the aromatic C—H stretching centered at 3060 cm^{-1} is attributed to small aromatic molecules such as caffeine, and phenolic acids such as chlorogenic acid, caffeic acid, and coumaric acid;[60] the asymmetric and symmetric CH_2 and CH_3 stretching modes at 2959, 2920, 2887, and 2851 cm^{-1} are linked to the caffeine and the lipidic part of coffee; the C═O stretching at 1736 cm^{-1} is attributed to the fatty acids present in the coffee; the C═O and C═C stretching modes between 1640 and 1510 cm^{-1} are due to the lignin and phenolic acid structures; the peaks 1450, 1377, and 893 cm^{-1} are assigned to the β-linkage of cellulose, and the C—O and C—O—C stretching modes between 1238 and 1028 cm^{-1} are due to the presence of the polysaccharides, monosaccharides, and phenolic compounds present in the coffee.[60–64]

In the CSF/P biocomposites, the spectra display overlapped peaks of the isolated components of the pure CSF and *P. ostreatus*. However, moving from the ratios 1:1 to 1:5, the intensity of the C═O stretching of the fatty acid present in the coffee decreases. As we move to the CSF/P 1:5 sample, the concentration of the mycelium component is higher, and probably more fatty acids are metabolized causing their reduced concentration in the final sample after growth. Moreover, the peak of the amide

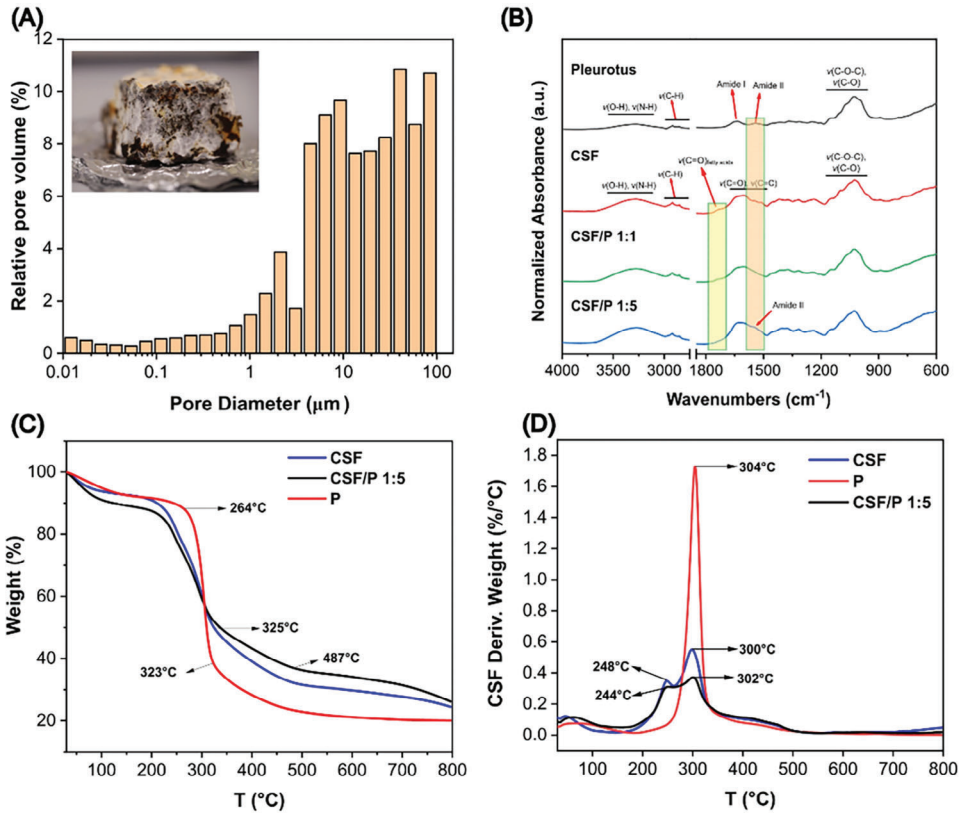

Figure 3. A) Pore size distribution measurement for the CSF/P biocomposites. B) ATR-FTIR spectra of the *P. ostreatus*, CSF, CSF/P 1:1, CSF/P 1:5 samples. The area of the C═O stretching of the fatty acids in the CSF and the Amide II stretching of the *P. ostreatus* proteins are highlighted by the yellow and red bars respectively. C) TGA thermograms and D) derivative thermogravimetric curves analysis of the CSF, *P. ostreatus*, and of the CSF/P 1:5 samples.

II (at 1541 cm^{-1}) typical of the mycelium protein, increases confirming a higher final concentration of the mycelium in these samples (Figure 3B; and Figure S1, Supporting Information). Overall, we can conclude that the pure mycelium and the CSF are both present in the biocomposites and that probably in the sample of a higher concentration of mycelium, the coffee is metabolized at a higher degree by the mycelium during its growth.

To evaluate the thermal degradation behavior of the CSF/P biocomposites in comparison with the individual components, thermogravimetric analysis (TGA) was performed as shown in Figure 3C,D. For all samples tested, the initial degradation step below 100 °C depicts the desorption of humidity. For the pure mycelium sample the small weight loss observed between 120 and 205 °C may be related to the degradation of polysaccharide side chains alone (such as α-glucans) or in glycoproteins, mainly branched glucomannan.[65] The main degradation step was observed between (200–325 °C) with a T_{max} at 304 °C prevalently attributed to the breakdown and volatilization of the polysaccharides backbone and especially of the β-glucans. Finally, the last degradation step observed in the range between 325 and 487 °C is related to the degradation of chitin-glucans and pure chitin.[65] On the other hand, for the CSF, two main degradation steps with T_{max} 248 and 300 °C were observed, Figure 3D. The step at T_{max} 248 °C is mainly attributed to the degradation of hemicellulose, while the second one, with T_{max} 300 °C, is attributed to the degradation of cellulose.[66] Concerning the CSF/P biocomposites, there are not extra degradation steps apart from those of pure mycelium and CSF, indicating that their interaction did not produce components that degrade earlier.

To determine the wetting properties of the developed mycelium biocomposites, water contact angle (WCA), and relative humidity measurements were performed. As shown in **Figure** 4A for all samples, the WCA values are around 114°, 122°, and 139°, with an increasing trend as the mycelium amount increases (i.e., the 1:5 biocomposite is the most hydrophobic), attributed to the hydrophobic nature of specific proteins (such as mannoproteins and hydrophobins) that can be found in the outermost layer of the fungal cell wall, and also to the micrometric roughness of the samples related to the fibrous nature of the developed systems.[55] This is further supported by the humidity adsorption study (Figure 4B). As shown, the values of the relative humidity adsorbed on the samples are very low (<20%) for all cases. However, the humidity adsorption decreases with increasing mycelium amount in the biocomposites, clearly indicating that upon its growth, the mycelium metabolizes the hydrophilic CSF into hydrophobic mycelium cell wall components.

To determine the mechanical strength of the developed biocomposites, compressive strength tests were conducted. The compressive strength of the mycelium-CSF samples depends on their porosity, pore size, material characteristics including the

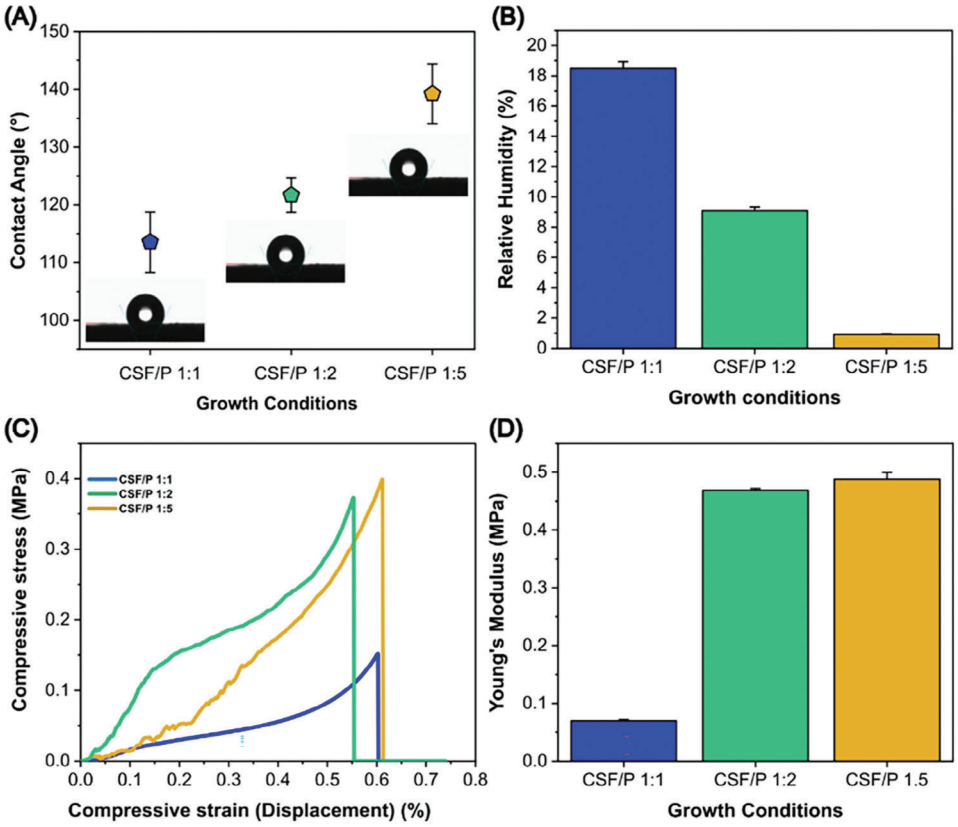

Figure 4. A) Static WCA measured on the CSF/P biocomposites. B) Humidity adsorption of the CSF/P biocomposites in the various growth conditions (CSF/P 1:1, 1:2, and 1:5). C,D) Mechanical characterizations: C) Compression strength, D) Young's modulus for the CSF/P biocomposites.

interaction of the CSF to the *P. ostreatus* mycelium, and on their density (0.066, 0.071, and 0.090 g cm^{-3} for CSF/P 1:1, 1:2, and 1:5, respectively). Figure 4C,D shows that CSF/P 1:5 samples display a higher compressive strength and compressive modulus when compared with the other two types of biocomposites (CSF/P 1:1 and 1:2). In particular, the Young's compressive modulus of the biocomposites is 0.06, 0.37, and 0.40 MPa, for the CSF/P 1:1, 1.2, and 1.5 samples, respectively (Figure 4D). The performance falls within the same range as other mycelium-bound composites of similar density, and is comparable with traditional synthetic insulation polymers. In particular mycelium composites containing fibrous dispersed, flax and hemp hurd, with slightly higher densities (0.099 and 0.094 g cm^{-3}, respectively) have shown Young's compressive moduli of 0.73 and 0.64 MPa,[67] respectively. Furthermore, conventional thermal and sound insulation products made from expanded polystyrene, with densities between ≈0.048 and 0.793 g cm^{-3} show a compressive strength between ≈0.02–2.50 MPa.[68] It should be mentioned that the biocomposites collapsed after reaching the nonreversible deformation, when the load on the compression tip was applied at a constant rate, reaching 55%, and 60% compressive strain.

2.1. Insulating Thermal and Acoustic properties

To evaluate the insulation capabilities of the developed samples, their thermal conductivity (TC) was measured. As can be seen in **Figure 5A**, the mean TC values of the biocomposites fall within the range of (0.03–0.04) Wm^{-1} K^{-1}, values representative of most of the insulation materials of natural or synthetic origin reported so far,[46] indicating their suitability for thermal insulation applications. In particular, mycelium-bound composites containing high-performance natural insulators, such as straw and hemp fibers present TC values between 0.04 and 0.08 Wm^{-1} K^{-1},[12] while conventional thermal insulation products, such as expanded polystyrene and glass wool present values of 0.03–0.04 Wm^{-1} K^{-1}.[12]

In Figure 5B is shown the transmitted sound energy derived from the sound tests conducted on the CSF/P samples. The results indicate that the biocomposite materials developed in this study exhibit a better acoustic insulation performance compared to a conventionally used acoustic insulation material (polyurethane foam) at all the frequency levels tested. In particular, from the results obtained, it can be deduced that both of the biocomposite samples tested (CSF/P 1:2, CSF/P 1:5) are promising for improved performance over the standard sound absorption system, especially in the region of 1000 Hz which is the critical frequency range for absorption of road noise. The CSF/P 1:1 composite was excluded from the sound test, due to its, above presented, poor mechanical properties. The performance of the other two biocomposite samples is similar and in accordance with what is reported in the literature for some other mycelium-agrowaste biocomposites that have been developed with different mycelium strains and agrowaste substrates.[12,41] In particular,

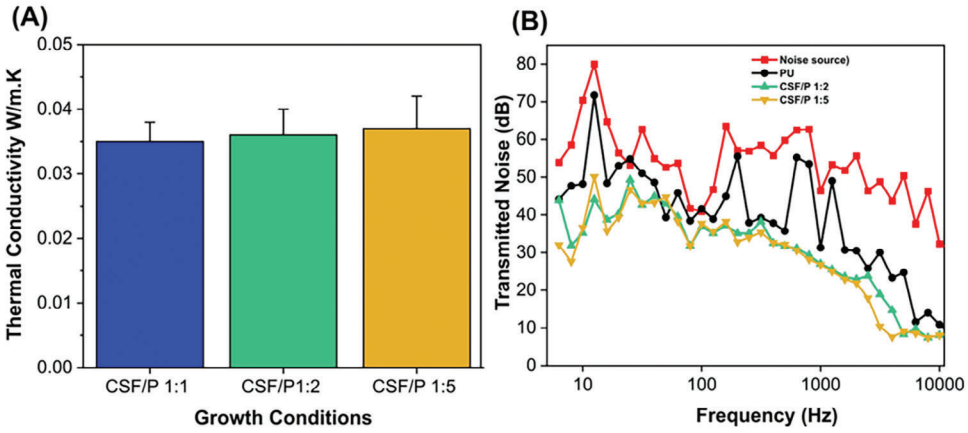

Figure 5. A) TC of CSF/P biocomposite samples. B) Sound absorption coefficient of the biocomposites compared to that of polyurethane foam. The data are based on an integrated speaker noise excitation (0–10000 Hz).

acoustic perception of road noise through mycelium-bound composites with fillers, such as rice straw-sorghum fiber, rice straw-cotton bur fiber, and sorghum fiber-switchgrass was reported in the range of 45.5–47.0 dB,[12,41] whereas the acoustic perception through CSF/P samples produced in this work was lower, in the range of 25.0–30.0 dB. Such performance is attributed to their porous and fibrous nature. In fact, the thin fibers in the mycelium biocomposites provide good acoustic absorption, acting as frictional elements since they can move easily resisting the acoustic wave motion and decreasing its amplitude.[41]

3. Conclusions

The successful development of novel agrowaste-based mycelium biocomposite materials has been achieved in this study. The biocomposites produced using CSF agrowaste substrate and *P. ostreatus* mycelium possess characteristic properties, such as low TC between 0.03 and 0.04 Wm^{-1} K^{-1}, and good acoustic isolation, which together with the thermal stability and hydrophobicity make them valuable candidates for biodegradable, thermal, and acoustic insulation materials in building and construction. The herein proposed systems can replace the conventional insulation and acoustic materials, such as glass or rock mineral wool, polyurethane, and extruded polystyrene foams, etc., with natural systems of low environmental impact. In fact due its self-growing nature, the system requires minimum energy consumption for its fabrication, while in the end of its lifespan it can be disposed in compost and treated as common organic waste.[27] This work paves the way to innovative solutions that prioritize eco-consciousness, aligning with the growing demand for greener and more sustainable solutions in the construction industry.

4. Experimental Section

Materials: Potato dextrose broth (PDB) (P6685) was purchased from Merck and used as growth medium. The *P. ostreatus* active culture was purchased from DSMZ, Germany, and maintained in a 100 mm Petri dish with PDB, transferring the culture to a fresh medium every 30 days. The coffee silverskin flakes (CSF) 0.3–1 cm in size were gently offered from Covim S.p.A., Genova, Italy. MilliQ water was used in all experimental activities.

Table 1. Labels and initial Agrowaste/Mycelium composition ratios (wt%), before the mycelium growth, of the different biocomposite samples.

Label	Agrowaste/mycelium composition ratio	CSF [wt%]	Mycelium [wt%]
CSF/P 1:1	CSF 10 g/P 10 g	50%	50%
CSF/P 1:2	CSF 10 g/P 20 g	33.33%	66.67%
CSF/P 1:5	CSF 10 g/P 50 g	16.67%	83.33%

Fabrication of the Biocomposites: The 3D mycelium-CSF biocomposites were fabricated following the scheme shown in Figure S2 (Supporting Information). First, the mycelium (*P. ostreatus*) was cultured in 2D form for 28 days in a PDB medium. The CSF flakes were grinded to decrease their size and sieved in order to obtain flakes with size ranging between 3 and few tens of micrometers and then dried at 40 ° C in an oven for 24 h. A 10 g of dried CSF powder was mixed with 10 mL of MilliQ water, and then sterilized in an autoclave (Systec VX-40, SN: 6050, Germany) at 121 °C for 1 h 30 min. Subsequently, 7 mm diameter punches of the mycelial inoculum were mixed with the CSF dispersion using a sterilized spatula under the biohazard hood (Angelantoni Life Science Srl, VBH 48 equipped with a 30 W germicidal ultraviolet lamp, wavelength 253.7 nm (UV-C)). The different initial weight ratios of CSF/mycelia are listed in **Table 1**. The mixtures were then placed in sterilized cubic-shaped ($5 \times 5 \times 5$ cm^3) silicone molds. The silicone molds were covered with sterile aluminum foils and placed inside a climatic chamber (Memmert HPP 260) to be incubated at controlled environmental conditions under dark for a period of one week at 27 °C and 78% ± 2% relative humidity (RH), to ensure stable growth of the mycelium biocomposite. During this period the growing mycelium was fed on the CSF, and colonized the organic substrate through the formation of interwoven 3D filamentous networks, into the shaped molds resulting in the formation of lightweight blocks ($4 \times 4 \times 3$ cm^3 in length, width, and height, respectively) of biocomposites in silicone mold. The biocomposites developed were then removed from the silicone mold, oven-dried at 40 °C for 10 h to deactivate the mycelium growth, and kept at room temperature for further characterization.

Morphological Characterization: To determine the morphology of the developed samples, digital photos were captured, using a Canon digital camera (Canon EOS 5D Mark II, DS126201, Japan). Scanning electron microscopy (SEM) analysis was conducted using a JEOL JSM 6490LA microscope at 10 kV accelerating voltage. For the observation, samples were sputter coated with a 10 nm thin gold layer (Cressington 208HR, Cressington Scientific Instrument Ltd., UK) and mounted on aluminum stubs, with a double-stick carbon tape.

Chemical Composition Analysis: The chemical composition and the possible chemical interactions of the components of the developed samples were studied using a single-reflection ATR accessory (MIRacle ATR, PIKE Technologies) coupled to an FTIR spectrometer (Equinox 70 FT-IR, Bruker). All spectra shown were averaged from 128 repetitive scans recorded from 4000 to 600 cm^{-1} with a resolution of 4 cm^{-1}. For the analysis, the dried blocks of the biocomposite material were pressed in a carver press (Model 3853CE Carver Inc. USA) for 5 min at 35 °C under a clamping force of 2 metric tons.

Density and Porosity: Skeletal density, i.e., the ratio of the mass of the solid to its volume excluding open and closed pores, was measured by helium pycnometry (Thermo Scientific Pycnomatic ATC). To do so, the dry samples (≈0.129 g of each sample) were placed in a 4 cm^3 cuvette and suspended in the pycnometer at 20.00 ± 0.01 °C, using helium as a measuring gas. The measurements were repeated ten times for each sample, and the accuracy was set to be ±0.001%.

The obtained skeletal density was then used to calculate the effective porosity and pore size distribution using MIP analysis (Thermo Fisher Scientific). Measurements were conducted using the low, Pascal 140 Evo, and high pressure, Pascal 240 Evo, modules, with mercury intrusion pressure ranges of 0.001–0.400 and 0.1–200.0 MPa, respectively. The data obtained from both porosimeters were combined and correlated to an equivalent pore size range of 0.01–100.0 µm using the S.OL.I.D. Evo Software. The pore size was calculated by the Washburn equation assuming a cylindrical and plate model, and a mercury contact angle and mercury surface tension of 140° and 0.48 N m^{-1}, respectively. For the measurement, the sample was rolled up in special support for membrane analysis and inserted in the dilatometer.

Water Interaction: An OCA 20 contact angle goniometer (DataPhysics, Instruments GmbH, Filderstadt, Germany) was used for defining the wettability of the samples at environmental conditions (room temperature: 18–20 °C and RH 60%). To assure a flat and uniform surface, the samples were pressed in a carver press (3853CE Carver Inc. USA) for 5 min at 35 °C under a clamping force of 2 metric tons. 5 µL droplets of deionized water were deposited on the samples' surface and the contact angle was calculated from the side view with the help of the instrument's software. For each sample, the measurements were carried out at five random locations of their surface, and their average values were presented. To determine the humidity adsorption efficiency, the samples were dried first at 105 °C for 4 h and then conditioned in a desiccator to remove any adsorbed humidity. The dried samples were then weighed on an electronic balance and then placed in a humidity chamber (RH 100%). After remaining in the humidity chamber for 9 days each sample was removed and weighed and the amount of adsorbed humidity was calculated as presented in Equation (1)

$$\text{Humidity Adsorption}\ (\%) = \frac{M2 - M1}{M1} * 100\% \quad (1)$$

Where M_1 is the initial dry mass and M_2 is the mass of the samples after the conditioning in the humidity chamber. During the 9 days of conditioning in the chamber the humidity was monitored using a Tinytag Ultra2 635 509 Hygrometer device.

Mechanical Characterization: The mechanical properties of the samples were determined by uniaxial test (compression test) on a dual-column universal testing machine Instron 3365 (Instron, Norwood, MA). The compression tests were carried out on the composite sample cubes (4 × 4 × 3 cm^3) using a 2 KN load cell. The compression strain rate was set to 10% min^{-1}. The compression modulus was determined from the slope of the initial linear region of the stress–strain curve. The test was performed at room temperature. For each growth condition (CSF/P 1:1, 1:2, and 1:5), five samples were tested, and the results were averaged to obtain a mean value. To ensure that all samples interact in the same way with the environmental humidity, before testing, they were conditioned in an oven at 40 °C for 6 h. Then they were brought to fixed environmental conditions of 18–20 °C and RH 60%, and all experiments were conducted at those conditions.

Thermal Characterization: The TC of the biocomposites was measured using a modified transient-plane source technique on a TC analyzer (C-Therm Technologies, TCi) following the ASTM D7984 test method. For the analysis, up to five measurements were performed for each sample. To ensure that all samples contain a similar amount of sorbed environmental humidity, the samples were adequately pretreated in the oven at 105 °C for 4 h and subsequently placed in a desiccator. Then they were brought to fixed environmental conditions of 18–20 °C and RH 60%, and all experiments were conducted at those conditions. In this way, differences in sorbed humidity amount attributed to the starting conditions were excluded. TGA on the samples was performed using a Q500 analyzer (TA Instruments, USA). 5–10 mg of the biocomposites, were placed into 100 µL platinum pans. Each one of the samples was heated at a rate of 10 °C min^{-1} from 30 to 800 °C under nitrogen atmosphere with flow rate of 50 mL min^{-1}.

Acoustic Test: The acoustic measurements were performed by a portable sound level meter (SLM) (type 01 dB Fusion, Acoem, France). The test container (a cubic PVC box) had external dimensions of 20 × 20 × 21 cm^3 and an opening of 5 × 5 cm^2 to which the biocomposite and reference test samples were fixed before the acoustic measurements. The biocomposite samples prepared for this test, had dimensions 10 × 10 cm^2, with a thickness of 2.4 cm. A flexible, open cell, polyurethane foam with an eggshell structure (skeletal density 1.17 ± 0.03 g cm^{-3}, highly interconnected pores, and mean pore size 148 ± 99 µm) with dimensions 12 × 12 cm^2, and a thickness of 2.5 cm, commonly used for sound absorption applications, was also tested as a reference sample. The test procedure was performed in several steps (see Figure S3 in the Supporting Information which gives a demonstration of the set up for the acoustic test): First, the speaker was switched on and placed inside the test container, then the testing sample was fixed in order to cover completely the opening of the container and the cubic box was sealed with a black magnetic tape. The SLM was then placed 12 cm away from the sample, pointed towards the source (0° incidence). Subsequently, audio playbacks of stored audio recording files at frequencies between 5 and 10 000 Hz, used as the sound source, were transmitted by the speaker. The sound tests involved measurements of the background noise level while the sound source is not operating, and the transmitted, though the polyurethane foam or composite samples, sound when the sound source is operating. All steps of sound transmission and recording have been performed through the control laptop and the FUSION wireless network. All experiments were conducted in environmental conditions (18–20 °C and RH 60%).

Supporting Information

Supporting Information is available from the Wiley Online Library or from the author.

Conflict of Interest

The authors declare no conflict of interest.

Data Availability Statement

The data that support the findings of this study are available from the corresponding author upon reasonable request.

Keywords

coffee silverskin, pleurotus ostreatus, porous biocomposites, self-growing materials, sustainability

Received: December 15, 2023
Revised: March 29, 2024
Published online:

[1] Programme, U. N. E., *Global Alliance for Building and Construction*, **2021**.
[2] L. Huang, G. Krigsvoll, F. Johansen, Y. Liu, X. Zhang, *Renewable Sustainable Energy Rev.* **2018**, *81*, 1906.
[3] P. F. Harmsen, M. M. Hackmann, H. L. Bos, *Biofuels, Bioprod. Biorefin.* **2014**, *8*, 306.
[4] M. Bonatti, P. Karnopp, H. Soares, S. Furlan, *Food Chem.* **2004**, *88*, 425.
[5] L. Cai, J. Tian, K. Feng, Y. Liu, Q. Jiang, *J. Non-Cryst. Solids* **2023**, *604*, 122136.
[6] L. H. Bell, D. H. Bell, *Industrial Noise Control: Fundamentals and Applications*, CRC Press, Boca Raton, FL **2017**.
[7] H. S. Seddeq, *Aust. J. Basic Appl. Sci.* **2009**, *3*, 4610.
[8] R. V. Gadhave, S. Srivastava, P. A. Mahanwar, P. T. Gadekar, *Open J. Polym. Chem.* **2019**, *9*, 39.
[9] K. M. Zia, H. N. Bhatti, I. A. Bhatti, *React. Funct. Polym.* **2007**, *67*, 675.
[10] S. Di Piazza, M. Benvenuti, G. Damonte, G. Cecchi, M. G. Mariotti, M. Zotti, *Recycling* **2021**, *6*, 40.
[11] V. Meyer, E. Y. Basenko, J. P. Benz, G. H. Braus, M. X. Caddick, M. Csukai, R. P. De Vries, D. Endy, J. C. Frisvad, N. Gunde-Cimerman, *Fungal. Biol. Biotechnol.* **2020**, *7*, 5.
[12] M. Jones, A. Mautner, S. Luenco, A. Bismarck, S. John, *Mater. Des.* **2020**, *187*, 108397.
[13] A. Javadian, H. Le Ferrand, D. E. Hebel, N. Saeidi, *SOJ Mater. Sci. Eng.* **2020**, *7*, 1.
[14] F. Razza, F. Degli Innocenti, A. Dobon, C. Aliaga, C. Sanchez, M. Hortal, *J. Cleaner Prod.* **2015**, *102*, 493.
[15] J. Michalak, S. Czernik, M. Marcinek, B. Michałowski, *Sustainability* **2020**, *12*.
[16] C. V. Vo, F. Bunge, J. Duffy, L. Hood, *Cell. Polym.* **2011**, *30*, 137.
[17] S. T. McKenna, T. R. Hull, *Fire Sci. Rev.* **2016**, *5*, 1.
[18] M. McCann, *Art J.* **1975**, *34*, 304.
[19] N. Grassie, *Polym. Degrad. Stab.* **1990**, *30*, 3.
[20] P. Dewick, M. Miozzo, *Futures* **2002**, *34*, 823.
[21] M. O. Yusuf, Z. M. Mohammed, A. A. Adewumi, M. T. Shaban, M. O. M. AlBaqawi, H. D. Mohamed, *Recycling* **2022**, *7*, 59.
[22] C. Ingrao, A. L. Giudice, J. Bacenetti, C. Tricase, G. Dotelli, M. Fiala, V. Siracusa, C. Mbohwa, *Renewable Sustainable Energy Rev.* **2015**, *51*, 29.
[23] O. Robertson, Fungal Future: A review of mycelium biocomposites as an ecological alternative insulation material. DS 101: Proceedings of NordDesign 2020, Lyngby, Denmark, 12th-14th August 2020 **2020**, 1.
[24] B. C. Almroth, S. E. Cornell, M. L. Diamond, C. A. de Wit, P. Fantke, Z. Wang, *One Earth* **2022**, *5*, 1070.
[25] C. Buratti, E. Belloni, E. Lascaro, F. Merli, P. Ricciardi, *Constr. Build. Mater.* **2018**, *171*, 338.
[26] J. Y. Choi, B. Y. Yun, Y. U. Kim, Y. Kang, S. C. Lee, S. Kim, *Environ. Pollut.* **2022**, *294*, 118616.
[27] J. K. Gan, E. Soh, N. Saeidi, A. Javadian, D. E. Hebel, H. Le Ferrand, *Sci. Rep.* **2022**, *12*, 19362.
[28] M. J. Carlile, in *The Growing Fungus* (Eds: N. A. R. Gow, G. M. Gadd), Springer, Dordrecht **1995**.
[29] M. E. Antinori, L. Ceseracciu, G. Mancini, J. A. Heredia-Guerrero, A. Athanassiou, *ACS Appl. Bio. Mater.* **2020**, *3*, 1044.
[30] M. Haneef, L. Ceseracciu, C. Canale, I. S. Bayer, J. A. Heredia-Guerrero, A. Athanassiou, *Sci. Rep.* **2017**, *7*, 41292.
[31] M. E. Antinori, M. Contardi, G. Suarato, A. Armirotti, R. Bertorelli, G. Mancini, D. Debellis, A. Athanassiou, *Sci. Rep.* **2021**, *11*, 12630.
[32] M. Ruggeri, D. Miele, M. Contardi, B. Vigani, C. Boselli, A. I. Cornaglia, S. Rossi, G. Suarato, A. Athanassiou, G. Sandri, *Front. Bioeng. Biotechnol.* **2023**, *11*, 1225722.
[33] J. Wang, Z. Huang, Q. Jiang, H. Roubík, Q. Xu, M. Cai, K. Yang, P. Sun, *Trends Food Sci. Technol.* **2023**, *138*, 628.
[34] N. Ivanova, in *Fungal Biopolymers and Biocomposites*, Springer, Singapore **2022**, p. 209–251.
[35] E. Karana, D. Blauwhoff, E.-J. Hultink, S. Camere, *Int. J. Des.* **2018**, *12*, 119.
[36] S. Manan, M. W. Ullah, M. Ul-Islam, O. M. Atta, G. Yang, *J. Bioresour. Bioprod.* **2021**, *6*, 1.
[37] L. Jiang, D. Walczyk, G. McIntyre, *A New Process for Manufacturing Biocomposite Laminate and Sandwich Parts Using Mycelium as a Binder*, ASC 2014 Proceedings San Diego, CA **2014**, p. 8.
[38] R. Abhijith, A. Ashok, C. Rejeesh, *Mater. Today Proc.* **2018**, *5*, 2139.
[39] X. Zhang, J. Hu, X. Fan, X. Yu, *J. Cleaner Prod.* **2022**, *342*, 130784.
[40] M. Jones, T. Bhat, C. H. Wang, K. Moinuddin, S. John, in *Proceedings of the 21st International Conference on Composite Materials, Thermal Degradation and Fire Reaction Properties of Mycelium Composites*, Xi'an, China **2017**, pp. 20–25.
[41] M. Pelletier, G. Holt, J. Wanjura, E. Bayer, G. McIntyre, *Ind. Crops Prod.* **2013**, *51*, 480.
[42] M. Pelletier, G. Holt, J. Wanjura, L. Greetham, G. McIntyre, E. Bayer, J. Kaplan-Bie, *Ind. Crops Prod.* **2019**, *139*, 111533.
[43] N. Walter, B. Gürsoy, *Biomimetics* **2022**, *7*, 100.
[44] R. E. Amaral, J. Brito, M. Buckman, E. Drake, E. Ilatova, P. Rice, C. Sabbagh, S. Voronkin, Y. S. Abraham, *Sustainability* **2020**, *12*, 5337.
[45] H. Schritt, S. Vidi, D. Pleissner, *J. Cleaner Prod.* **2021**, *313*, 127910.
[46] P. P. Dias, L. B. Jayasinghe, D. Waldmann, *Results Mater.* **2021**, *10*, 100189.
[47] E. Bayer, G. McIntyre, Method for producing grown materials and products made thereby, Google Patents, **2016**.
[48] M. M. Aranda-Calipuy, A. Roncal-Lázaro, M. A. Quezada-Alvarez, R. Siche, L. Cabanillas-Chirinos, W. Rojas-Villacorta, S. M. Benites, S. Rojas-Flores, *Sustainability* **2023**, *15*, 9157.
[49] D. Lingam, S. Narayan, K. Mamun, D. Charan, *Constr. Build. Mater.* **2023**, *391*, 131841.
[50] L. Yang, D. Park, Z. Qin, *Front. Mater.* **2021**, *8*, 737377.
[51] H. Mbabali, M. Lubwama, V. A. Yiga, E. Were, H. Kasedde, *J. Inst. Eng.: Ser. D* **2023**, *105*, 97.
[52] C. Girometta, A. M. Picco, R. M. Baiguera, D. Dondi, S. Babbini, M. Cartabia, M. Pellegrini, E. Savino, *Sustainability* **2019**, *11*, 281.
[53] F. V. Appels, S. Camere, M. Montalti, E. Karana, K. M. Jansen, J. Dijksterhuis, P. Krijgsheld, H. A. Wösten, *Mater. Des.* **2019**, *161*, 64.
[54] B. Slováčková, L. Lloyd, *Acta Facultatis Xylologiae Zvolen* **2021**, *63*, 5.
[55] M. Haneef, L. Ceseracciu, C. Canale, I. S. Bayer, J. A. Heredia-Guerrero, A. Athanassiou, *Sci. Rep.* **2017**, *7*, 41292.
[56] É. M. dos Santos, L. M. de Macedo, L. L. Tundisi, J. A. Ataide, G. A. Camargo, R. C. Alves, M. B. P. Oliveira, P. G. Mazzola, *Trends Food Sci. Technol.* **2021**, *111*, 280.
[57] A. Nolasco, J. Squillante, S. Velotto, G. D'Auria, P. Ferranti, G. Mamone, M. E. Errico, R. Avolio, R. Castaldo, T. Cirillo, *J. Cleaner Prod.* **2022**, *370*, 133520.
[58] L. Lu, S. Tibpromma, S. C. Karunarathna, R. S. Jayawardena, S. Lumyong, J. Xu, K. D. Hyde, *Pathogens* **2022**, *11*, 411.
[59] A. Hejna, *Waste Manage.* **2021**, *121*, 296.
[60] Y. Chun, Y. G. Ko, T. Do, Y. Jung, S. W. Kim, U. S. Choi, *Colloids Surf., A* **2019**, *562*, 392.
[61] E. K. Kemsley, S. Ruault, R. H. Wilson, *Food Chem.* **1995**, *54*, 321.
[62] D. J. Lyman, R. Benck, S. Dell, S. Merle, J. Murray-Wijelath, *J. Agric. Food Chem.* **2003**, *51*, 3268.
[63] K. Pandey, *J. Appl. Polym. Sci.* **1999**, *71*, 1969.
[64] M. Contardi, D. Kossyvaki, P. Picone, M. Summa, X. Guo, J. A. Heredia-Guerrero, D. Giacomazza, R. Carzino, L. Goldoni, G. Scoponi, *Chem. Eng. J.* **2021**, *409*, 128144.

[65] C. Girometta, D. Dondi, R. Baiguera, F. Bracco, D. Branciforti, S. Buratti, S. Lazzaroni, E. Savino, *Cellulose* **2020**, *27*, 6133.
[66] C. Del Pozo, J. Bartrolí, S. Alier, N. Puy, E. Fàbregas, *Waste Manage.* **2020**, *109*, 19.
[67] E. Elsacker, S. Vandelook, J. Brancart, E. Peeters, L. De Laet, *PLoS One* **2019**, *14*, e0213954.
[68] G. Bumanis, P. P. Argalis, G. Sahmenko, D. Mironovs, S. Rucevskis, A. Korjakins, D. Bajare, *Recycling* **2023**, *8*, 19.